



Slurry aluminizing mechanisms of Ni-based superalloys incorporating an electrosynthesized ceria diffusion barrier



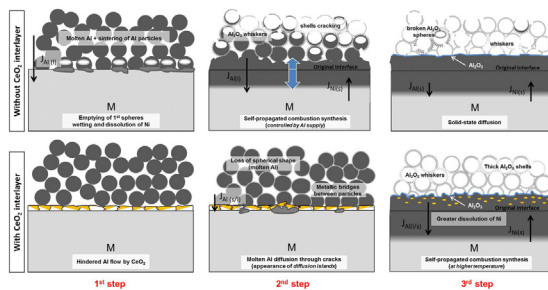
Baptiste Bouchaud*, Benoit Rannou, Fernando Pedraza

Laboratoire des Sciences de l'Ingénieur pour l'Environnement LaSIE FRE-CNRS3474, Université de La Rochelle, Pôle Sciences et Technologie, Avenue Michel Crépeau, 17042 La Rochelle cedex 01, France

HIGHLIGHTS

- New slurry-sintered TBC system incorporating an electrosynthesized ceria interlayer.
- Growth mechanisms and intermetallic formation elucidated by SEM/EDS, 3D-DSC and TGA.
- Selective diffusion barrier ability of ceria demonstrated to limit Cr upward diffusion.
- Thicker β -NiAl coating obtained by delayed Al diffusion and enhanced Ni outward diffusion.
- Thicker crusts of alumina spheres and greater sintering of the Al_2O_3 shells evidenced with ceria.

GRAPHICAL ABSTRACT



ARTICLE INFO

Article history:

Received 16 March 2013

Received in revised form

16 September 2013

Accepted 18 September 2013

Keywords:

Coatings
Intermetallic compounds
Oxides
Interfaces
Diffusion
Sintering

ABSTRACT

This study investigates the effect of an electrosynthesized ceria interlayer on the growth mechanisms of a full TBC system sintered from a slurry containing spherical Al micro-particles. A potential Selective Diffusion Barrier (SDB) ability of the ceria interlayer appears. It is demonstrated that ceria allows the Al enrichment of the substrate while limiting the Cr upward diffusion and segregation of Al_xCr_y . It is found that the ceria interlayer partially hinders the flow of solid and molten Al into the substrate at 700 °C from the spheres. Simultaneously, the flow of Al among the spheres results in the establishment of bridges and in the loss of sphericity all by maintaining a metallic core. In contrast, emptying of the particles and quick formation of $\delta\text{-Ni}_2\text{Al}_3$ rapidly occur in the absence of ceria interlayer. Increasing the annealing temperature to 1100 °C for 2 h brings about the formation of a β -NiAl coating thicker than the one obtained without an interlayer and promotes thicker crusts and a greater sintering of the Al_2O_3 shell of the particles. This is proposed to result both from delayed Al inward diffusion and enhanced Ni outward diffusion promoted by the heat release accompanying the exothermic formation of the Ni_xAl_y phases.

© 2013 Elsevier B.V. All rights reserved.

1. Introduction

Conventional thermal barrier coating (TBC) systems for the hottest sections of aero-engines operating in harsh conditions at high temperature rely on the use of Pt-modified aluminide bond-coats with an yttria partially stabilized zirconia (YSZ) thermal insulating topcoat [1–5]. The use of very expensive platinum and low yield of YSZ EB-PVD processing restricts their likely

* Corresponding author. Tel.: +33 (0) 5 46 45 86 00; fax: +33 (0) 5 46 45 82 41.

E-mail addresses: baptiste.bouchaud01@univ-lr.fr, bbouch01@univ-lr.fr (B. Bouchaud), brannou@univ-lr.fr (B. Rannou), fpedraza@univ-lr.fr (F. Pedraza).

Table 1

Nominal chemical composition of the investigated Ni-based superalloy substrates (wt.%).

	Ni	Cr	Co	Mo	W	Ta	Al	Ti	Other
René N5	62	7	8	2	5	7	6		0.2 Hf, 3.0 Re
CM247	62	8	9	0.5	9	3	6	0.7	1.4 Hf

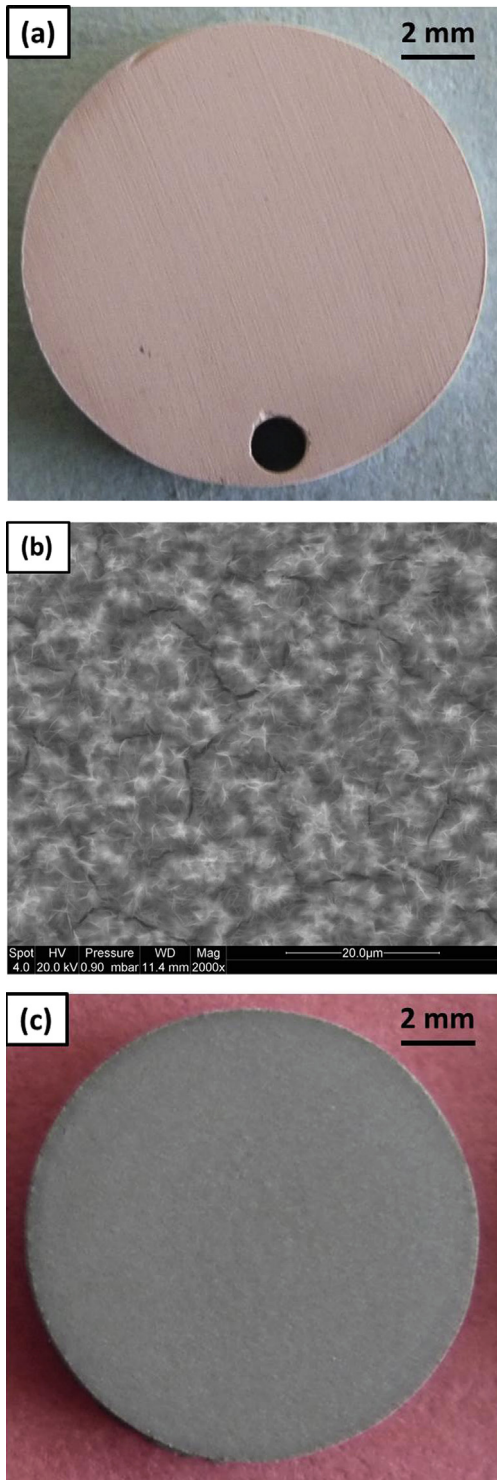


Fig. 1. (a) Macroscopic and (b) SEM top view of the model nickel substrate after electrodeposition of ceria-based layer and air drying onto which (c) the slurry coating is applied by air spraying.

extrapolation to lower temperature engine sections where single aluminide coatings are mostly employed. However, the required increase of the turbine inlet temperature to improve the thermodynamic yield of the engine raises new considerations for low pressure turbine components and more economically viable coating approaches offering a low environmental impact are thus sought.

Among them, the new approach studied within the PARTICOAT program [6] using water-based slurries incorporating micro-sized Al particles [7] referred to the simultaneous formation upon an appropriate heat treatment of a full TBC system consisting of (i) an aluminium diffused bondcoat and (ii) an intermediate thermally grown oxide to which (iii) an insulating topcoat of alumina hollow spheres was attached to. From an experimental standpoint, previous works reported on both the formation and the degradation mechanisms of such coating systems obtained on model nickel [8–10], martensitic steels [11] and Ni-based superalloy and austenitic steel substrates [12–14] for various application purposes at high temperature.

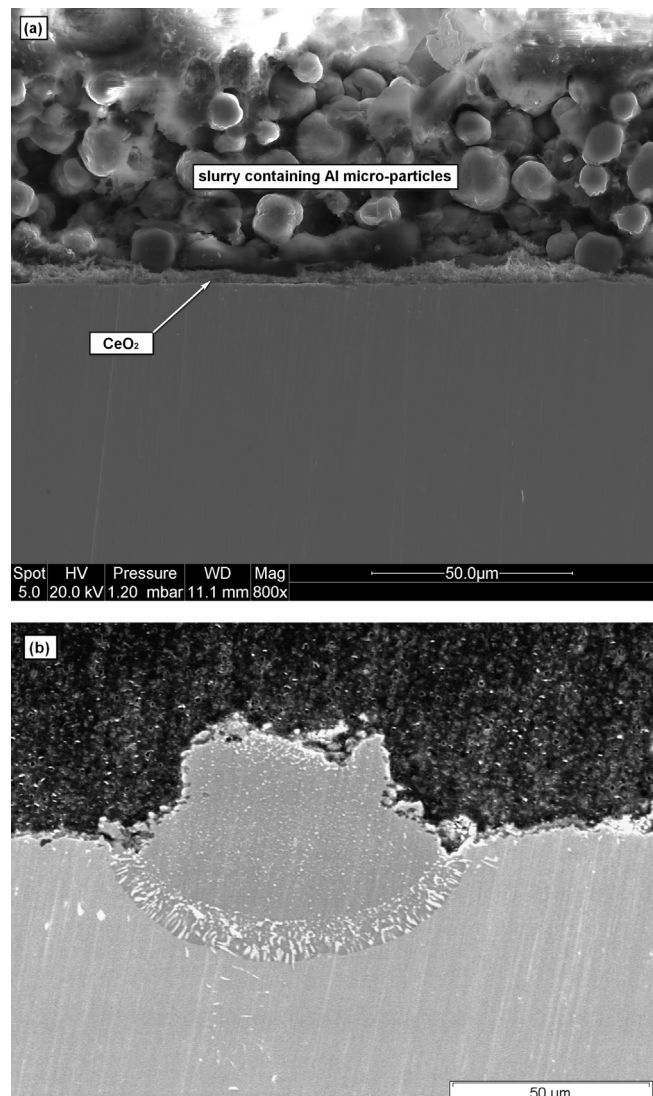


Fig. 2. SEM cross-section morphology of (a) uncured slurry-coating showing its good uniformity and wetting properties over the as-deposited CeO_2 interlayer and of (b) diffusion islands and detachment of the topcoat onto cured slurry ($700^\circ\text{C}/2\text{ h} + 1100^\circ\text{C}/2\text{ h}$, Ar) with an annealed ceria interlayer ($1050^\circ\text{C}/1\text{ h}$, Ar).

Pedraza et al. [8] showed that the quick Al ingress firstly occurred by nickel dissolution into molten Al, the diffusion being likely amplified by self-propagating combustion synthesis (heat release accompanying the exothermic formation of Ni_xAl_y intermetallic phases) upon the continuous Al supply from the micro-particles [15]. Thereafter, a step at higher temperature led to the formation of the β -NiAl phase by nickel outward diffusion. Using the same approach, strong correlations between more complex substrate chemistries and the resulting microstructure and composition of the coating were described [12]. However, few works have emphasized the influence of the Cr content in Ni-based superalloys [13] and Ni20Cr model substrate [16] even though Cr tends to segregate in NiAl due its low solubility in this phase [17]. Indeed, Rannou et al. [16] showed that Cr promoted the detachment of the topcoat of alumina spheres and the appearance of Kirkendall porosity between the coating and the substrate due to the formation of chromium aluminides that impede further Al inward diffusion as also observed in high activity pack aluminizing processes [18].

More recently, an electrodeposited cerium oxide interlayer clearly demonstrated the ability to both limit the inward diffusion of Al and the outward diffusion of Cr during the oxidation of a conventional low activity out-of-pack aluminide onto a René N5 Ni-based superalloy at 1100 °C and to restrain the formation of SRZ [19]. Based on these promising results, the present work therefore intends to study the potential dual beneficial effect of an electro-synthesized ceria Selective Diffusion Barrier (SDB) for slurry aluminizing of Ni-based substrates, expected to (i) reduce

chromium upward diffusion and to (ii) promote even aluminized diffused layers.

2. Experimental

René N5 and CM247 Ni-based superalloy substrates, whose nominal chemical compositions are given in Table 1, were studied in the present work. Coupon samples of 12 mm diameter and of 2 mm thick were grit blasted with 220 mesh alumina particles and cleaned with ethanol under ultrasonic agitation before any other experimental step. Commercially available polycrystalline nickel model substrate (99.98%, Goodfellow) coupons of 12.7 mm of diameter and 2 mm of thickness were also used as baseline to elucidate the mechanisms of formation. The nickel coupons were ground with #180 SiC paper grade and cleaned following the same experimental protocol.

The ceria coatings were generated by cathodic electrodeposition in a three-electrode set-up from 0.1 M concentrated cerium-nitrate fresh solutions at an applied current density of -1 mA cm^{-2} for a deposition time up to 20 min [20]. After elaboration, the deposits were rinsed in ethanol and dried with hot air ($T > 50^\circ\text{C}$) to release free water and stored for at least 24 h in a desiccator with silica gel. The samples were then aluminized by air spraying a controlled mass of 9 mg cm^{-2} of slurry on the samples surface [8]. The Particoat slurry contains 45 wt.% of Al micro particles dispersed in 55 wt.% binder (1:10 PVA: H_2O in weight). After drying for at least 1 h in ambient air [7], a subsequent diffusion annealing treatment was performed under flowing argon gas (700°C for 2 h followed by

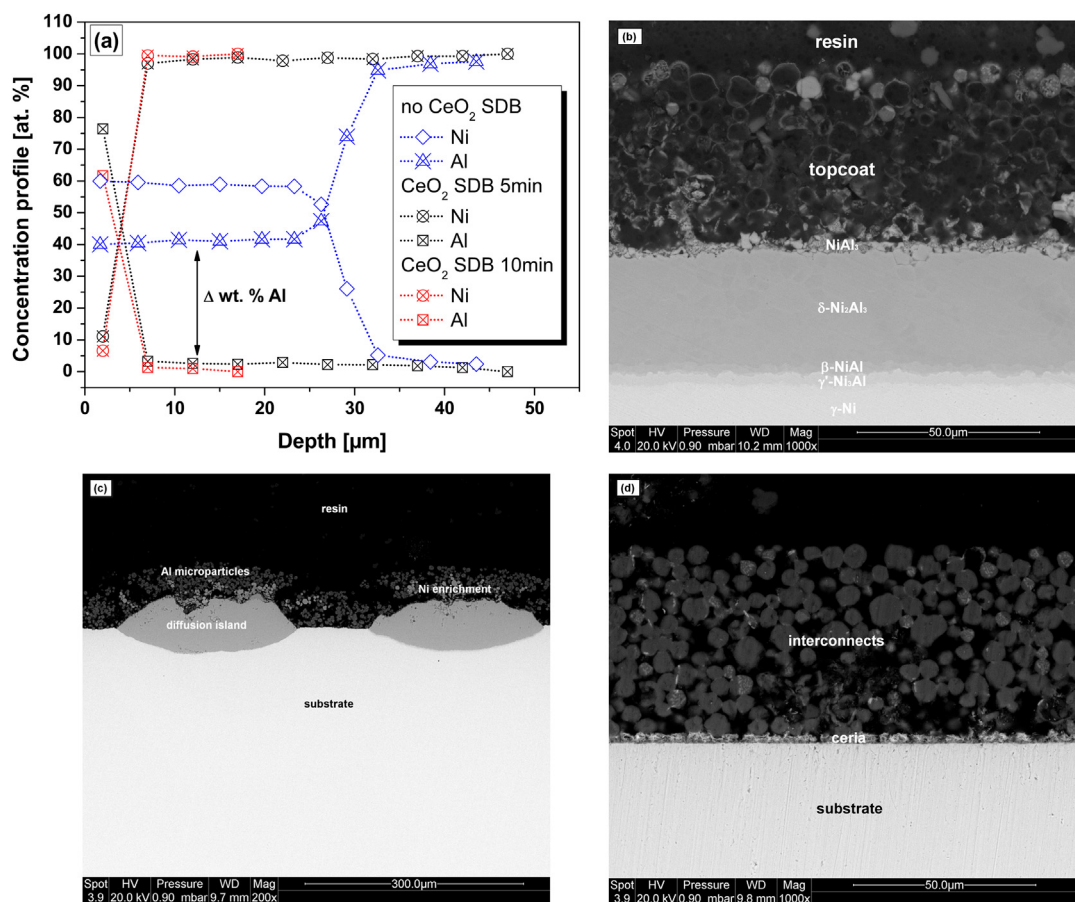


Fig. 3. Comparison of the features of the slurry coatings after annealing at 700 °C for 2 h. (a) EDS composition profiles. General view of the cross-sections: (b) without ceria and (c, d) with a ceria SDB interlayer generated for 5 min and 10 min of deposition, respectively.

1100 °C for 2 h with a heating rate of 5 °C min⁻¹ and a cooling rate of 50 °C min⁻¹) to promote simultaneously the sintering of the Al particles and the formation of a β-NiAl bondcoat [8–10].

The coated samples were systematically characterized by X-ray diffraction in the Bragg-Brentano mode using a Bruker AXS D8 Advance (λ_{Cu}) in combination with Scanning Electron Microscopy coupled to EDS analyses (SEM/EDS, FEI Quanta 200F/EDAX and JEOL 5410LV/Rontec) for top view/cross-section observations and concentration profiles, respectively. High precision DSC measurements were also carried out with a SETARAM LabSys Evo TGA-DSC device using a 3D sensor configuration in order to understand the effect of the presence of a ceria interlayer on the diffusion and growth mechanisms of the slurry coating. SDB-free and SDB-coated substrates were heated into a platinum crucible with an alumina lining up to 1100 °C at 10 °C min⁻¹ under flowing argon gas atmosphere to prevent from strong signals coming from likely oxidation phenomena.

3. Results and discussion

3.1. Tailoring the ceria SDB coating: compatibility with the slurry

Fig. 1a shows a macrograph of the ceria-coated model nickel substrate in the as-deposited conditions after drying. At the naked eye, the deposit exhibits a white colour accounting for Ce(OH)₃ formation [21] and fully covers the surface of the substrate. Characterization by SEM (Fig. 1b) also indicates that the deposit presents a network of relatively thin cracks that develop during the thickening of the layers [20] and is expected to favour the Al enrichment by offering preferential diffusion pathways with the substrate. After application of the slurry on the interlayer by air spraying, the coverage appears to be homogeneous (Fig. 1c).

The cross-section characterization confirms the good continuity and wetting of the water-based slurry containing micro-sized Al particles on the ceria-based film (Fig. 2a). This is indeed promoted by the very nature of the electrodeposited layers, which have been quoted to soak easily water till saturation due to their porous and multi-cracked structure [20] and to their composition (oxy-hydroxide) that promotes the adsorption and bonding of water [22]. In contrast, stabilization of the stoichiometric CeO₂ fluorite form by annealing (1050 °C/1 h, Ar) [21] brings about the early detachment of the slurry upon curing below 400 °C because of the limited adsorption of water on stoichiometric ceria compounds [23]. As a result, random diffusion islands and the detachment of the topcoat (Fig. 2b) occur after the full annealing of the slurry (700 °C/2 h + 1100 °C/2 h, Ar). The fast desorption of free water amplified by the melting and decomposition of the PVA binder [7] explains such phenomenon and therefore annealed stoichiometric ceria interlayers have not been retained further in the study.

3.2. Composition and microstructure of the slurry aluminide onto pure nickel

After heat treatment at 700 °C for 2 h, the thickness of the diffusion layer reaches about 35–40 µm (Fig. 3a). Simultaneously, the sintering of the particles is promoted (interconnected spheres are observed) and they got emptied (Fig. 3b), thus suggesting that most of the Al has been supplied to the substrate. From the topcoat/diffused layer interface to the nickel substrate, combined SEM/EDS and X-ray diffraction suggested the formation of (i) a thin and brittle NiAl₃ outermost layer (ii) the Ni₂Al₃ main intermetallic phase and (iii) an inner interdiffusion area composed of two sub-layers of decreasing Al content, i.e. β-NiAl and γ'-Ni₃Al. The quick growth of such coatings has been studied in detail by Pedraza et al. [8].

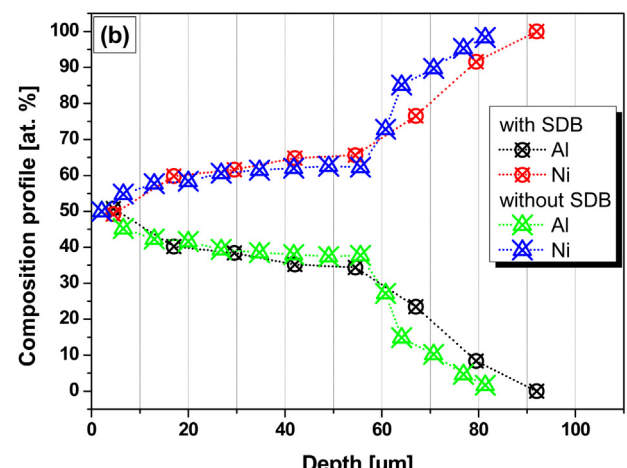
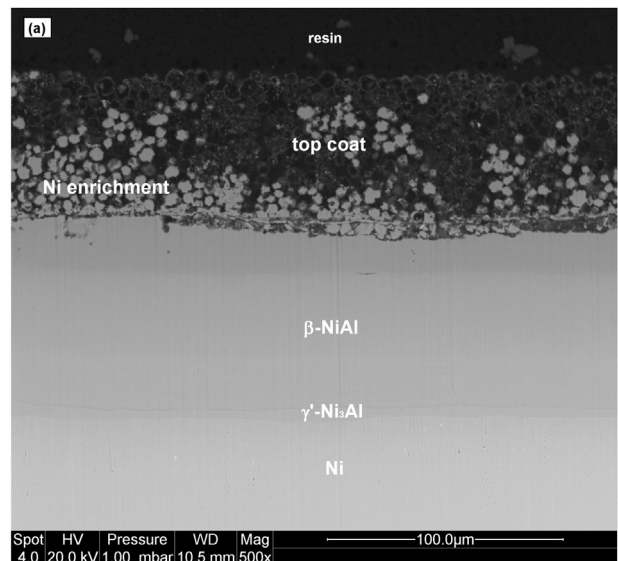


Fig. 4. Typical (a) cross-section morphology of a slurry-coated model nickel substrate with a ceria SDB interlayer and (b) comparison of the EDS concentration profiles for Al and Ni with a SDB-free slurry-coated Ni after diffusion/annealing treatment under argon gas flow (700 °C/2 h + 1100 °C/2 h).

In contrast, the presence of a ceria layer seems to regulate the Al diffusion flow (Fig. 3c and d). When the SDB is thin (5 min of deposition, 2.5 ± 0.2 µm thick), random islands of Al diffused into nickel appear (Fig. 3c) and seem to form in a similar manner than in

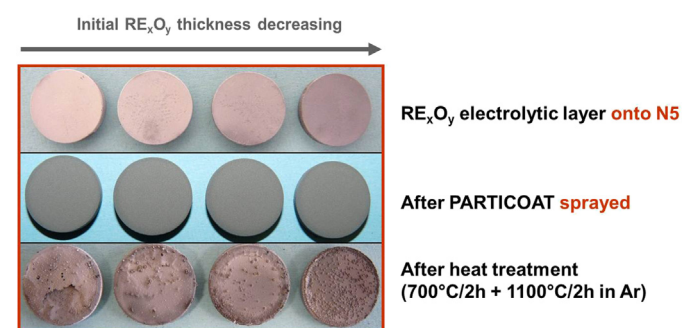


Fig. 5. Macroscopic top view of the generated slurry coatings after heat treatment (700 °C/2 h followed by 1100 °C/2 h, Ar) as a function of the initial thickness of the ceria SDB interlayer.

the ceria-free nickel substrates, i.e. contact of Al with Ni followed by dissolution of Ni into molten Al over the original surface of the substrate [8]. However, in the areas with a more compact ceria film, Al is physically impeded to react with nickel and the eutectic reaction of Al + NiAl₃ at 639 °C cannot occur [24]. By increasing the thickness of the ceria interlayer (10 min of deposition, 5 ± 0.5 µm thick), flattening of the particles started to occur by melting of the Al contained in the spheres upon annealing at 700 °C for 2 h (Fig. 3d). However, little Al incorporated into the Ni substrate (Fig. 3a) although aluminization of ceria-free pure nickel was reported to occur after only 1 h at 600 °C [9]. It derives that the electrodeposited ceria interlayer prevents the direct contact of the Al spheres with nickel in an effective manner and impedes the eutectic reaction. Therefore, the ceria interlayer can be considered as a Selective Diffusion Barrier (SDB).

Based on the work reported by Pedraza et al. [8], higher temperature of 1100 °C was required to stabilize a fully transformed α-Al₂O₃ topcoat and a diffused β-NiAl phase similar to conventional TBCs. However, in the presence of the ceria SDB, thicker alumina shells and further incorporation of nickel into the spheres of the topcoat than in SDB-free samples occur [8]. The diffused β-NiAl layers are also thicker (75 µm) with the ceria SDB (Fig. 4a) than in its absence (60 µm) [8] but the composition profiles (Fig. 4b) are quite similar and suggest an Al-rich β-NiAl external layer and a γ'-Ni₃Al internal layer in contact with the substrate. The only differences

relates to the softer decrease of the Al content adjacent to the substrate in the presence of the ceria SDB, hence explaining the greater thickness of the coating. The X-ray diffraction patterns (not shown) confirmed unambiguously that the uppermost aluminide coating is composed of a main matrix of β-NiAl (with lower contribution of γ'-Ni₃Al) together with α-Al₂O₃ coming from the hollow spheres and from the thermally grown oxide (TGO) at the diffused layer/topcoat interface. Fingerprints of NiAl₂O₄ spinel phase are also evidenced by local Raman spot analyses within the topcoat due to the dissolution of Ni (NiO + Al₂O₃ = NiAl₂O₄) [25,26]).

3.3. Composition and microstructure of the slurry aluminide onto Ni-based superalloys

The influence of the initial ceria thickness (e.g. ranging from 5 µm to 20 µm) and of the inherent development of cracks during thickening of the layers has been investigated on slurry-coated René N5 superalloys. After spraying of the slurry, the coating appears again very homogeneous. However, upon annealing, the thin SDB layers resulted in a greater number of protuberances whereas cracking and spallation occurred with thicker ones (Fig. 5). According to the SEM/EDS and XRD measurements (not shown), none or random Al diffusion occurred into the substrate while additional oxide phases to Al₂O₃ grew (i.e. NiAl₂O₄ and NiO) by direct

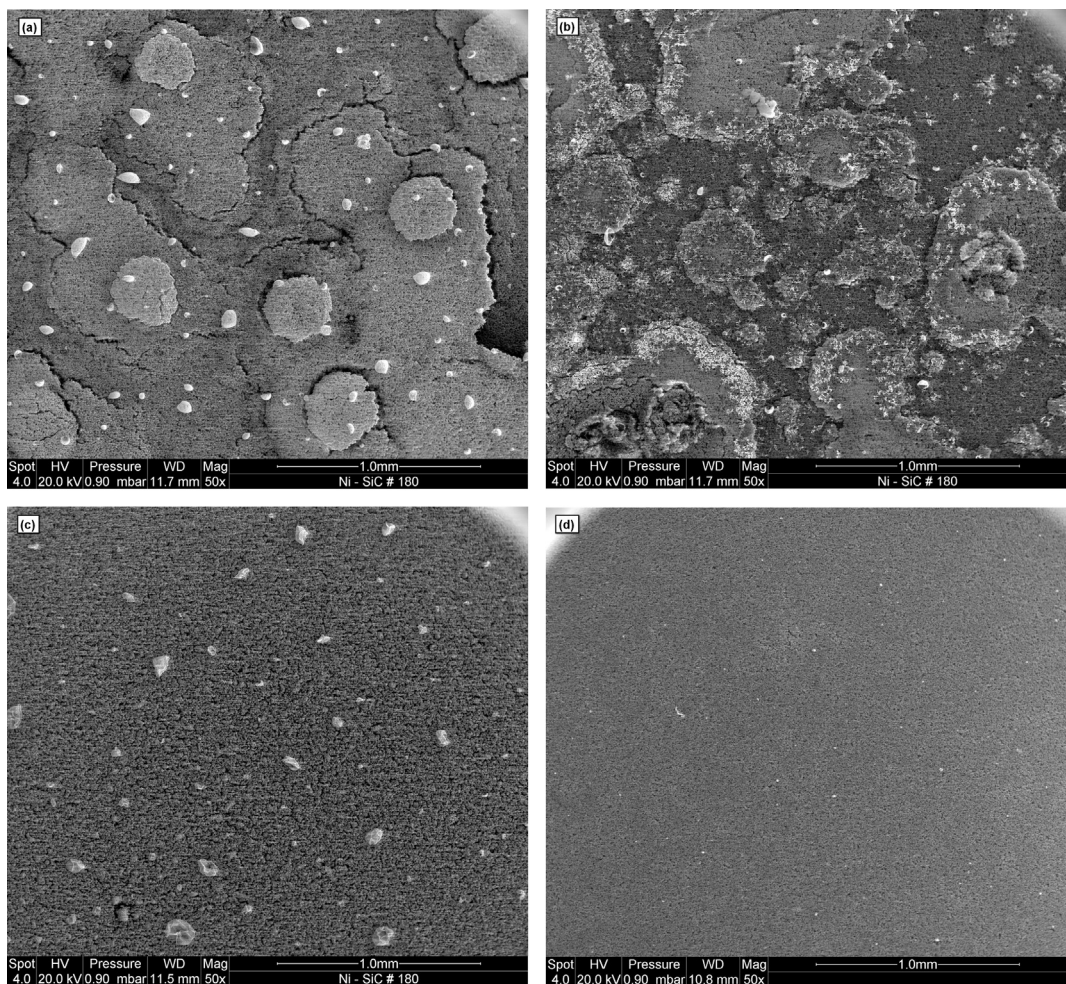


Fig. 6. SEM top surface micrographs after the slurry-applied Particoat after thermal treatment (700 °C/2 h + 1100 °C/2 h, Ar) with a ceria SDB (a) 20 min/12 µm, (b) 15 min/8 µm, (c) 10 min/5 µm and (d) comparison with a ceria SDB-free coating.

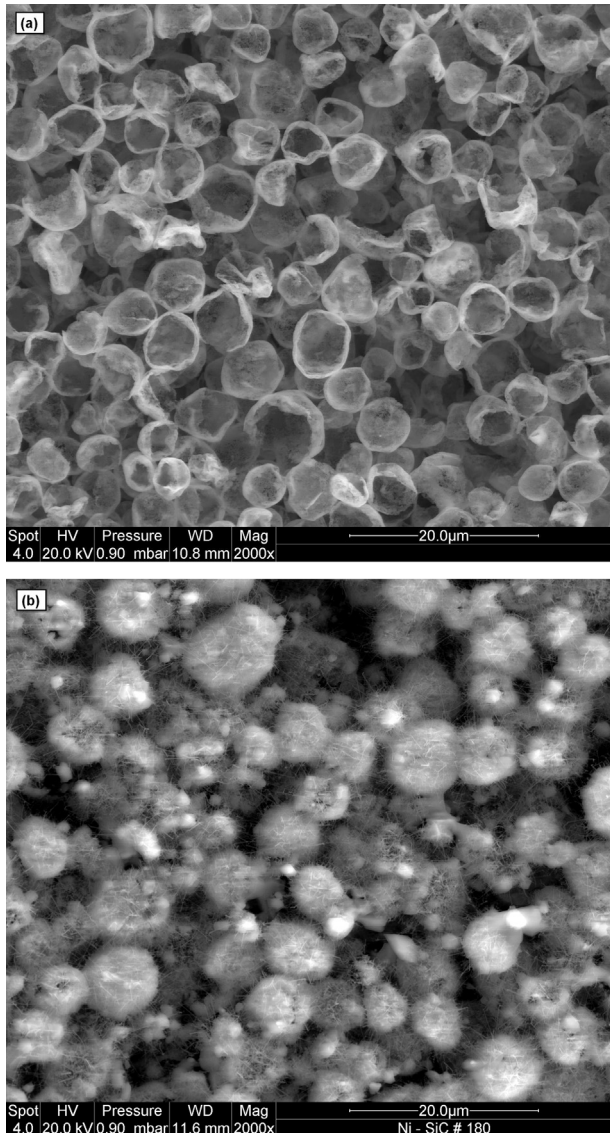


Fig. 7. Morphology of the oxidized spheres within the topcoat (a) without and (b) with ceria SDB.

oxidation of the raw substrate and of the Ni-rich topcoat. Further inspection of the spalled topcoat also revealed a low sintering of the particles and metallic Al remains in the spheres [10].

The original features (microstructure and thickness) of the interlayer appear therefore to be critical during the diffusion/annealing treatment. Consequently, the optimum thickness of the SDB interlayer for these experiments seems to range between 5 μm and 10 μm (case of Section 3.2). The SEM/EDS observations gathered in Fig. 6 confirmed that the thinner the initial SDB thickness, the lower the number of cracks observed within the topcoat but the greater the number of protuberances (Fig. 5). However, the size of the protuberances increases with SDB thickness (Fig. 6a and b) since cracking of ceria occurs [21]. Therefore, the top surface morphology in thin ceria interlayers (Fig. 6c) is rather similar to ceria SDB-free systems (Fig. 6d). The experimental evidence to confirm such hypothesis will be discussed thereafter.

At higher magnification, various microstructural differences between the oxidized spheres of the topcoat (Fig. 7) appear when comparing the absence or the presence of the ceria interlayer. In the former, the hollow particles appear broken but well sintered and

the shells exhibit the typical morphology of the $\alpha\text{-Al}_2\text{O}_3$ with some whiskers [8]. In the latter, the oxidized particles also seem well sintered but maintain the spherical shape and are fully covered with very fine whiskers. Such “whisker-like” morphology is believed to result from the greater Al content in the spheres, which cannot diffuse because of the presence of the ceria interlayer. Indeed, the increase of temperature results in the simultaneous melting of Al and in the shrinkage of the oxide shell that lead to cracks and pores [14,27]. Therefore, molten Al can flow through these defects and oxidise immediately in contact with any oxidising species (O_2 and H_2O contained in the Ar (g)). Due to the limited partial pressures of oxygen in the argon flow, only the most thermodynamically stable $\alpha\text{-Al}_2\text{O}_3$ form can grow as confirmed by the absence of any metastable alumina using XRD and micro-Raman spectrometry.

Inspection of the cross-section confirmed that the particles are well sintered and that the oxide shells are thicker (Fig. 8a) in the presence of the SDB than in its absence (Fig. 8b). Ni also incorporates to the hollow particles in a greater extent when a SDB layer is present (Fig. 8a and X-ray map of Fig. 9), hence bringing about a relative depletion in Ni from the underlying $\beta\text{-NiAl}$ layer (compare EDS profiles of Fig. 8c and d). The diffused layers are also thicker (100 μm) with a SDB layer than without. Therefore, it seems that the ceria SDB impedes Al inward diffusion but fosters Ni outward diffusion. The O and Al enrichment at the interface between the topcoat and the diffusion layer appears in both cases and has been associated with a $\alpha\text{-Al}_2\text{O}_3$ TGO [8,11,12]. However, in the presence of the SDB, Ce mainly incorporates to such interface making the outward flow of chromium to be arrested underneath (Fig. 9). Therefore neither Kirkendall porosity nor incorporation of Cr to the topcoat occurs as opposed to the SDB-free slurry coatings [16].

3.4. Slurry coating formation: mechanisms involved and influence of the ceria SDB interlayer

In order to better understand the mechanisms involved during the growth of the slurry coating and the influence of a ceria interlayer, both thermal gravimetry (TGA) and differential scanning calorimetry (DSC) experiments were carried out. The resulting curves obtained during the annealing of the slurry coatings on SDB and SDB-free pure nickel and nickel superalloys (René N5 and CM247) are presented on Fig. 10 a and b, respectively. The analysis and identification of all the peaks are gathered in Table 2.

The overall shape of the TGA curves (Fig. 10a) is similar to those reported by Rannou et al. when applying the same thermal treatment to similar PVA + H_2O + Al micro-particles free-standing slurry but using a different experimental set-up [7]. A continuous mass loss occurred till 550 °C (Fig. 10a, zone I) due to the successive melting (235 °C) and decomposition of the PVA binder and to the Al dehydroxylation (460 °C) and the formation of the amorphous Al_2O_3 . All the thermal events identified in [7] could not be evidenced in our case due to very weak signal close to the detection limit of our device using a 3D configuration set-up. The crystallization of the $\gamma\text{-Al}_2\text{O}_3$ phase at higher temperature is accompanied by a light mass gain ascribed to the onset of oxidation phenomena (zone II) before melting of Al ($T_m = 660$ °C). Thereafter, a progressive increase of the temperature till 1100 °C leads to a sharp increase of the mass gain (zone III) associated with higher oxidation kinetics and to the polymorphic transformation of transient aluminas into the stable alpha phase above 1000 °C [28] after which the mass gain slows down.

However, some differences are observed in the DSC curves (Fig. 10b), in particular for the zone II. Indeed, in the free-standing slurry, Rannou et al. [7] clearly demonstrated the presence of one

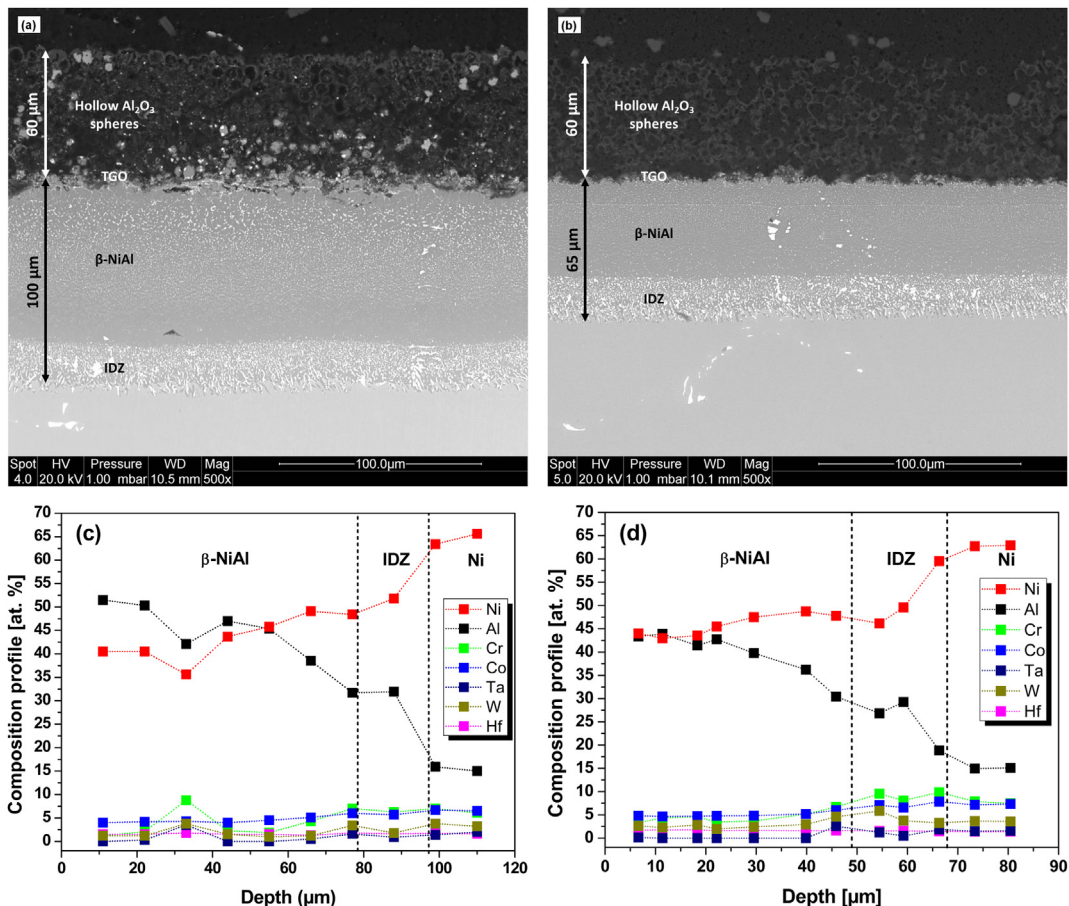


Fig. 8. Features of the coating after annealing at 700 °C/2 h + 1100 °C/2 h. Cross-section (a) with and (b) without a ceria interlayer and (c) and (d) the corresponding EDS profiles.

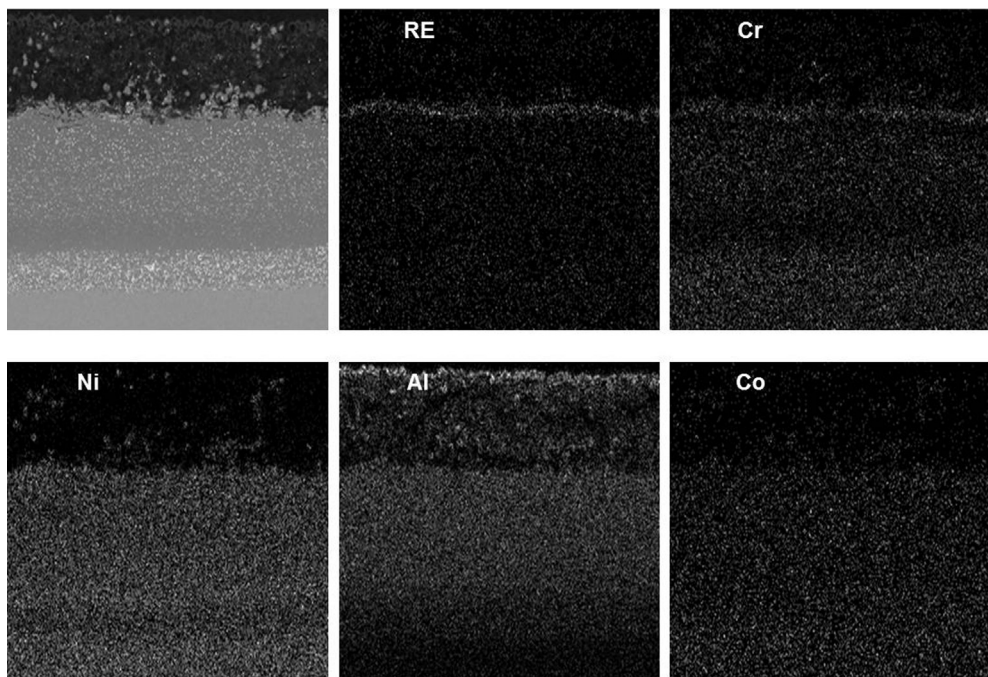


Fig. 9. SEM cross-section and X-ray maps of the Particoat coating deposited onto René N5 with a ceria SDB interlayer showing how Cr is impeded to incorporate into the topcoat.

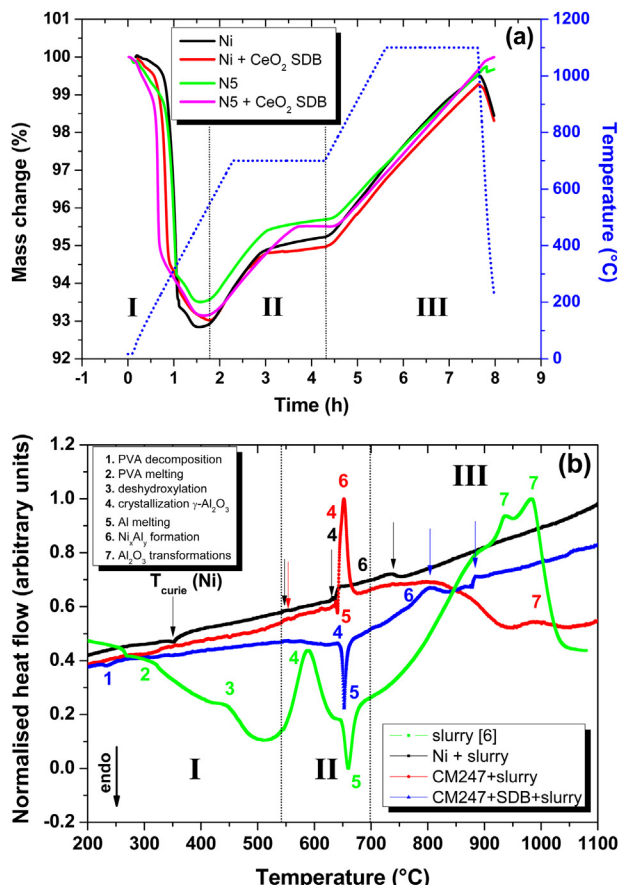


Fig. 10. (a) TGA curves of the slurry-coated pure nickel and N5 superalloy and (b) DSC curves of the slurry-coated pure nickel and CM-247 superalloy with and without ceria SDB interlayer during the heat treatment (700 °C/2 h + 1100 °C/2 h). The DSC curve of free-standing slurry from Rannou et al. [6] is included for comparison purposes.

wide exothermic peak related to the crystallization of the amorphous alumina (peak 4) followed by one endotherm (peak 5) corresponding to the melting of Al at about 660 °C. Further exothermic variations at higher temperatures were then ascribed to the polymorphic transformations of alumina accompanied by a strong positive drift of the DSC signal due to the exothermic oxidation effect. When the slurry is then applied onto a metal substrate (pure Ni or a Ni-based superalloy) in the absence of a ceria SDB, the temperatures of transformations are altered. Indeed, the crystallization of the amorphous alumina phase occurs at temperatures closer to the melting point of Al (peak 4). In addition, the melting of Al (peak 5) shifts to lower temperatures on pure nickel because of either the appearance of the eutectic (Al + Al₃Ni) phase at 639 °C, or the presence of impurities such as Si [15] or Cr [29] that lower the melting temperature, or both. For the Ni-based superalloy, the temperature at which peak 5 appears is slightly higher (541 °C)

probably because of the presence of various alloying refractory elements. Yet, for both the nickel and the superalloy substrates, this endotherm is unambiguously overlapped by one additional strong exotherm (peak 6) associated with the formation of intermetallic compounds (Ni_xAl_y) grown by high temperature self-propagating combustion synthesis [15] once Al is put in contact with nickel [8]. Therefore, the greater heat release registered in the superalloy compared to pure nickel promotes the more exothermic formation of Ni₂Al₃ [30] as the main intermetallic phase. Since Al is mostly consumed by diffusion into the substrate, the positive drift of the DSC signal ascribed to the oxidation of Al at higher temperature is much lower than in a free-standing slurry [7], where all the Al particles are subjected to oxidation.

The most remarkable DSC results are found when a ceria SDB layer is applied between the substrate and the slurry. Indeed, although the endotherm associated with the Al melting (peak 5) appears at a temperature close to the one recorded for the free-standing slurry, the strong exotherm (peak 6) related to Ni_xAl_y intermetallic formation vanished. This suggests that the formation of intermetallic phases does not occur or is delayed, a phenomenon confirmed in Fig. 3c and d where very limited diffusion of Al into the substrate was observed. With more Al available in the topcoat, further exothermic behaviour appears over a wide temperature range (730 °C–841 °C) that can be related to the oxidation of the Al particles and thicker crusts were thus observed (Fig. 8a).

4. Summary

On the basis of the above results, the formation of the slurry coating and the impact of the presence of a ceria SDB layer can be summarized into three main stages described in Fig. 11. In essence, the ceria SDB strongly modifies the diffusion mechanisms and delays the growth of the intermetallic phases by preventing the direct contact of the Al spheres with nickel (stage 1). Indeed, whereas emptying of the first spheres and wetting and dissolution of Ni occurs onto SDB-free substrate (Fig. 11a) already after 1 h at 600 °C onto pure nickel [9], the diffusion of Al is delayed for the SDB-coated substrate (Fig. 11d). However, softening and/or melting of the Al spheres occur by the effect of temperature and/or temperature depressants that bring about a loss of spherical shape. The Al flow ensures the interconnection between the particles, hence the sintering of the topcoat whether in the presence or in the absence of the ceria SDB.

At 700 °C, emptying of the particles and quick formation of Ni₂Al₃ rapidly occur in the absence of SDB (Fig. 11b). Thereafter, solid-state diffusion controls the growth of the coating (Fig. 11c) [15]. For the SDB-coated substrate, the eutectic reaction can only take place in local areas where the ceria layer is micro-cracked (stage 2), thus leading to uneven diffused islands that grow over the initial surface of the substrate (Fig. 11e). This phenomenon is less marked for the thinner interlayers than for the coarser ones for which higher temperatures are required for aluminizing (stage 3). The higher temperature triggers in turn further Al diffusion and

Table 2

Summary of the main thermal events obtained by DSC measurements.

System	Temperature of thermal transformations (°C)						
	PVA		$\gamma\text{-Al}_2\text{O}_3$		Al melting		Ni _x Al _y formation
	$T_{\text{peak}} \text{ melting}$	$T_{\text{range}} \text{ decomposition}$	$T_{\text{onset}} \text{ crystallization}$	T_{peak}	T_{range}	T_{peak}	T_{range}
Free-standing slurry [6]	220	240–360	589	660	647–680	—	—
Slurry-coated Ni	235	251–328	632	637	—	645	638–753
Slurry-coated CM247	235	251–328	638	641	—	652	641–820
SDB slurry-coated CM247	235	251–328	641	652	644–667	803	730–841

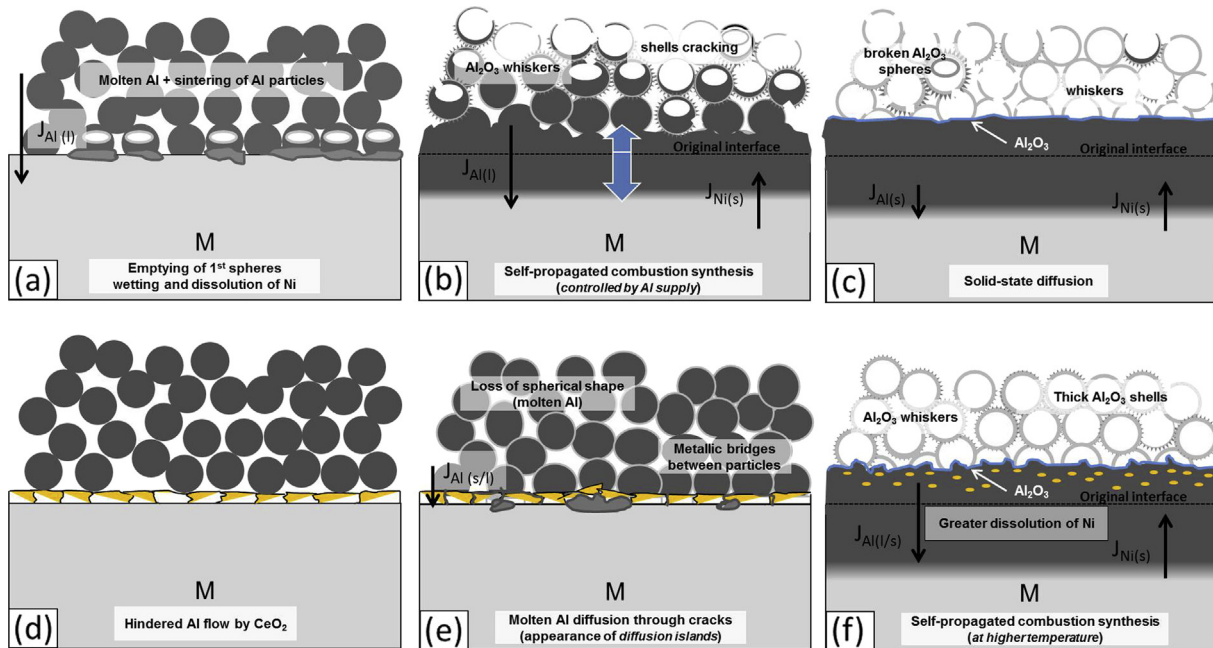


Fig. 11. Schematic of the three main stages involved in the formation of the aluminide coatings on nickel substrates from the slurry (a, b, c). Modification of aluminizing mechanisms by the presence of a ceria SDB interlayer (d, e, f). N.B.: J is the flux, M is the metal substrate.

much greater oxidation and sintering of the spheres. Therefore, the particles can maintain their spherical shape and develop whiskers from the Al available in the core of the particles (Fig. 11f). Overall, delayed Ni dissolution into molten Al and enhanced outward diffusion of Ni at higher temperature may explain the growth of thicker β -NiAl diffused coatings amplified by self-propagated combustion synthesis [15] as far as metallic Al is supplied.

5. Conclusions

The selective diffusion barrier ability of an electrosynthesized ceria interlayer has been demonstrated to allow slurry-aluminizing of Ni-based superalloy while limiting the Cr upward diffusion. This specific design therefore constitutes a promising way for slurry-aluminizing higher Cr-containing Ni-based superalloys in order to prevent from topcoat detachment due to the development of Kirkendall porosity. The specific features of the ceria interlayer (cracks, thickness...) appeared to be critical on the interfacial diffusion/growth mechanisms to obtain a beneficial effect. It appeared that with adequate (10 μm thick) ceria layer, the Al flow into the substrate is delayed or limited and higher temperatures are required to trigger the onset of Al diffusion and to enhance the outward diffusion of Ni. As confirmed by DSC, the exothermal Ni_xAl_y formation could then result from self-propagated combustion synthesis that led to thicker diffused β -NiAl layers than in the absence of a ceria SDB layer and a well sintered topcoat exhibiting thicker alumina crusts but incorporating greater amount of NiAl_2O_4 spinel phase.

Acknowledgements

This study was supported under the programme PARTICOAT FP7-NMP-LARGE-211329 (2008–2012) funded by the European Union.

References

- [1] G.W. Goward, D.H. Boone, *Oxid. Met.* 3 (1975) 475–495.
- [2] J.A. Nesbitt, E.J. Vinarcik, C.A. Barrett, J. Doychak, *Mat. Sci. Eng. A* 153 (1992) 561–566.
- [3] G.W. Goward, *Surf. Coat. Technol.* 108 (1998) 73–79.
- [4] J.R. Nicholls, *MRS Bull.* 28 (2003) 659–670.
- [5] M.P. Taylor, R.D. Jackson, H.E. Evans, *Mat. High Temp.* 26 (2009) 317–323.
- [6] www.particoat.eu (accessed to March 2013).
- [7] B. Rannou, F. Velasco, S. Guzman, V. Kolarik, F. Pedraza, *Mat. Chem. Phys.* 134 (2012) 360–365.
- [8] F. Pedraza, M. Mollard, B. Rannou, J. Balmain, B. Bouchaud, G. Bonnet, *Mat. Chem. Phys.* 134 (2012) 700–705.
- [9] G. Bonnet, M. Mollard, B. Rannou, J. Balmain, F. Pedraza, X. Montero, M. Galetz, M. Schütze, *Defect Diff. Forum* 323 (2012) 381–386.
- [10] M. Mollard, B. Rannou, B. Bouchaud, J. Balmain, G. Bonnet, F. Pedraza, *Corr. Sci.* 66 (2013) 118–124.
- [11] V. Kolarik, M.M. Juez-Lorenzo, M. Anschustegui, H. Fietzek, *Mater. Sci. Forum* 595 (2008) 769–777.
- [12] X. Montero, M. Galetz, M. Schütze, *Surf. Coat. Technol.* 206 (2011) 1586–1594.
- [13] B. Rannou, B. Bouchaud, J. Balmain, G. Bonnet, F. Pedraza, *Oxid. Met.* (2013), <http://dx.doi.org/10.1007/s11085-013-9427-6>.
- [14] X. Montero, M. Galetz, M. Schütze, M. Mollard, B. Rannou, B. Bouchaud, V. Kolarik, G. Bonnet, F. Pedraza, 8th Int. Symp. On High Temperature Corrosion and Protection of Materials (HTCPM2012), Les Embiez, France, 2012.
- [15] M. Galetz, X. Montero, M. Mollard, M. Günthner, F. Pedraza, M. Schütze, *Intermetallics* 44 (2014) 8–17.
- [16] B. Rannou, M. Mollard, B. Bouchaud, J. Balmain, G. Bonnet, V. Kolarik, F. Pedraza, *Defect Diff. Forum* 323 (2012) 373–379.
- [17] A. Chien, D. Gan, P. Shen, *Mater. Sci. Eng. A* 206 (1996) 215–224.
- [18] P. Moretto, J. Bresser, D.J. Arrell, *Mater. Sci. Eng. A* 272 (1999) 310–320.
- [19] B. Bouchaud, B. Rannou, F. Pedraza, Electrosynthesized oxide-based selective diffusion barrier interlayer for slurry-applied PARTICOAT aluminising of nickel-based superalloys, in: European Workshop – New Approaches to High Temperature Coatings, Lanzarote, Spain, 2012.
- [20] B. Bouchaud, J. Balmain, G. Bonnet, F. Pedraza, *Electrochim. Acta* 88 (2013) 798–806.
- [21] B. Bouchaud, J. Balmain, G. Bonnet, F. Pedraza, *Appl. Surf. Sci.* 268 (2013) 218–224.
- [22] M. Brossard, B. Rannou, B. Bouchaud, J. Balmain, G. Bonnet, F. Pedraza, *Oxid. Met.* (2013), <http://dx.doi.org/10.1007/s11085-013-9426-7>.
- [23] B. Bouchaud, J. Balmain, L. Barrere, T. Delannoye, F. Pedraza, *Corr. Sci.* 68 (2012) 176–185.
- [24] H. Okamoto, *J. Phase Equil. Diff.* 25 (2004) 394.
- [25] D.F. Susan, A.R. Marder, *Oxid. Met.* 57 (2002) 159–180.
- [26] P. Saltykov, O. Fabrichnaya, J. Golczewski, F. Aldinger, *J. Alloys Compd.* 381 (2004) 99–113.
- [27] V. Kolarik, M. Del Mar Juez-Lorenzo, H. Fietzek, *Mat. Sci. Forum* 696 (2011) 290–295.
- [28] N.N. Sirota, G.N. Shokhina, *Kristall und Technick* 9 (1974) 913–919.
- [29] E. Rosell-Laclau, M. Durand-Charre, M. Audier, *J. Alloys Compd.* 233 (1996) 246–263.
- [30] D. Shi, B. Wen, R. Melnik, S. Yao, T. Li, *J. Solid State Chem.* 182 (2009) 2664–2669.